

DOI: 10.54503/0571-7132-2022.65.4-475

PHOTOMETRIC AND SPECTROSCOPIC ANALYSIS OF THE SX Phe STAR BL Cam

M.ABDEL-SABOUR, M.I.NOUH, A.SHOKRY, G.M.HAMED,
H.A.ISMAIL, A.TAKEY, S.A.ATA, I.ZEAD

Received 30 May 2022

Accepted 11 November 2022

In the present paper, we report the photometric and spectroscopic observations of the pulsating star BL Cam obtained by the 1.88 m telescope at the Kottamia astronomical observatory (KAO). Fourier analysis of the light curves indicates one frequency, 25.14427 c/d, with harmonics 51.112 c/d, 33.388 c/d, and 17.72464 c/d. The frequency of 31-32 c/d reported in the literature is not detected in our data except for one close to 33.3882934 c/d. A total of 55 new times of maximum light have been presented. A new value of $(1/P) dP/dt$ is estimated using the O-C diagram based on all newly obtained times of maximum light combined with those taken from the literature, assuming the periods are decreasing and changing smoothly. Using model atmosphere analysis, we computed the effective temperature and surface gravity as $T_{\text{eff}} = 7625 \pm 300$ K and $\log g = 4.30 \pm 0.37$. The bolometric magnitude $M_{\text{bol}} = 2.335$, radius $R = 1.69 R_{\odot}$, luminosity $L = 0.957 L_{\odot}$, the mass $M = 1.68 M_{\odot}$, and pulsation constant $Q = 0.025$ days. Locations of the star on the $M-R$ and $M-L$ diagrams indicate that it is close to the ZAMS track and is an unevolved star.

Keywords: *stars: variables: SX Phe stars: frequency and pulsation analysis: model atmosphere analysis*

1. *Introduction.* SX Phoenicis (SX Phe) stars are typically found in the galaxy's outer regions, known as the galactic halo. Their luminosity changes over 1-2 hours and have short periods (≤ 0.08 day) and large amplitudes (> 0.3 mag). In globular clusters, they are mostly found among blue stragglers [1]. These stars exhibit short-period pulsation behavior that varies on time scales ranging from 0.03 to 0.08 days (0.7 to 1.9 hours). SX Phe stars have spectral classifications in the A2-F5 range and magnitude differences of up to 0.7.

Giclas et al. [2] discovered BL Cam (= GD 428 in Simbad, 2MASS J03471987+6322422, Gaia DR2 487276688415703040), which was thought to be a candidate for a white dwarf. It is a pulsating star with a period of 0.039 days and an amplitude of 0.33 mag, according to Berg & Duthie [3]. McNamara [4] classified it as a Population II star with a metal abundance of $[Fe/H] = -2.4$. Previous researchers have investigated its multiperiodic character [5-7]. Hintz et al. [8] measured 32.679 c/d for the first overtone and 0.783 for the period ratio of the first overtone to the fundamental mode. Previous authors [9-12] had also

discovered the first overtone at 31.6 c/d, resulting in a period ratio of 0.810. On the other hand, the first overtone did not detect [7]. In a multi-site photometric investigation of BL Cam, 21 distinct pulsation frequencies (excluding the fundamental mode) with amplitudes ranging from 1.6 to 7.4 mmag were discovered [6].

As demonstrated by [1], the period content of BL Cam is dominated by 25.5790 ± 3 c/d and its two harmonics and an independent frequency of 25.247 ± 2 c/d. An analysis of their times of maxima from the literature [13] determined a periodic change that made BL Cam a binary system and demonstrated that the evolution of the ephemerides of the different authors was natural and correct, given the shortness of the available data at their times. They showed that a binary system causes long-term variation with a longer time horizon.

In the present paper, we carried out photometric and spectroscopic observations for the star BL Cam. We will use a model atmosphere to determine the star's effective temperature and surface gravity at different phases. Frequency analysis, O-C curve, and period change of the star are investigated. The structure of the paper is as follows. The photometric analysis is presented in section 2. The spectral analysis is described in section 3. Section 4 is devoted to determining the star's physical parameters and evolution state, and the conclusion reached is presented in section 5.

2. Photometric analysis.

2.1. *Observation and data reduction.* We present new photometric observations of BL Cam by using the 1.88m telescope of the Kottamia Astronomical Observatory (KAO), Egypt. We applied data reduction, bias subtraction, and flat-field correction to the raw CCD images without dark subtraction, which was already negligible. All observations were taken using an EEV 42-40 CCD camera with a format of 2048 x 2048 pixels, cooled by liquid nitrogen to -120 C°. Fig.1

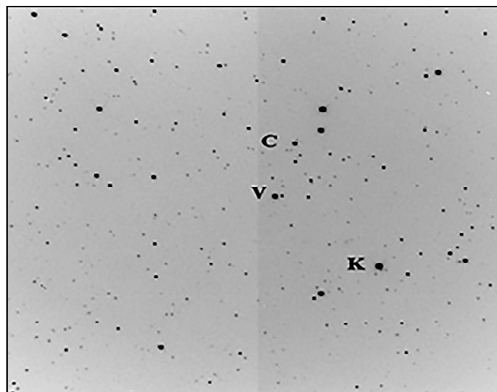


Fig.1. CCD image (8' x 8') of BL Cam taken with KFISP; the variable star is denoted as (V), the comparison star as (C), and the check star as (K).

shows the field BL Cam taken with the KAO. The variable star, the comparison star, and the check star are marked as V, C, and K, respectively. Fig.2 shows the KAO observations obtained in Johnson BVR filters and the SDSS in g , r , i , and z filters for the two nights, November 24 and November 26, 2021. All observations were analyzed using the MuniWin v.1.1.26 software [14], implementing the differential magnitudes method of aperture photometry.

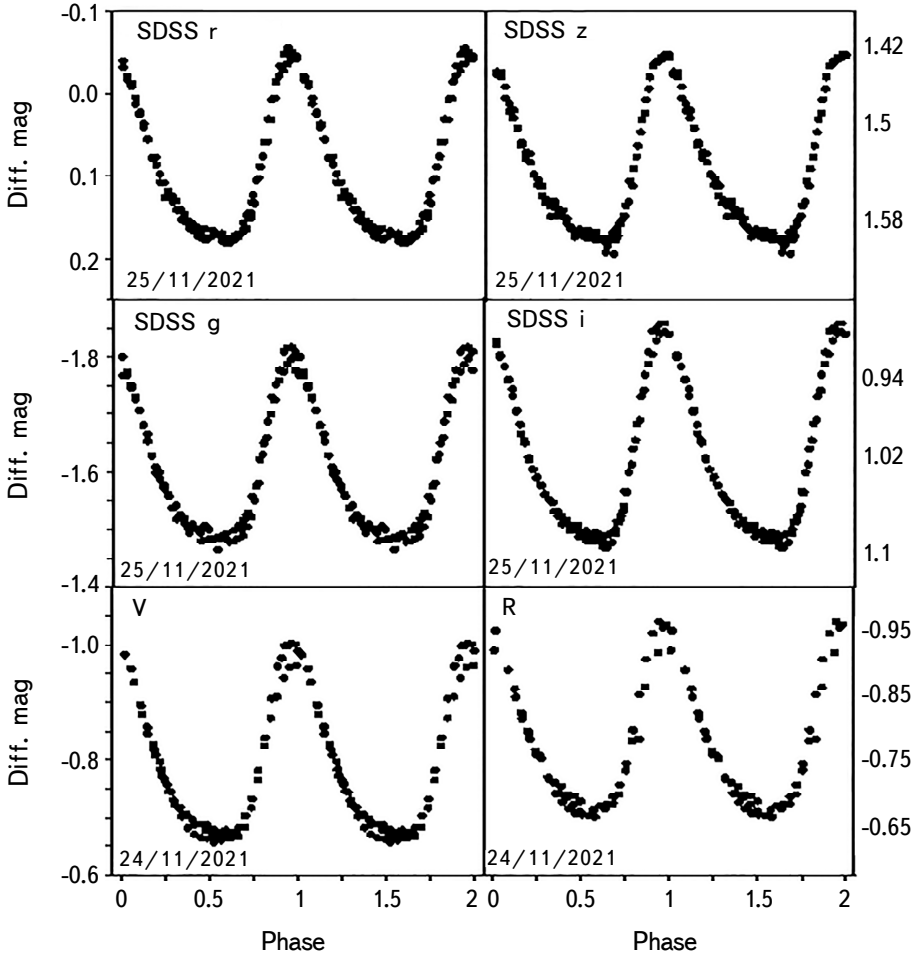


Fig.2. The differential magnitude of BL Cam; SDSS g , r , i , and z bands and VR bands.

2.2. Frequency and pulsation analysis. The frequency analysis of the BL Cam light curves was carried out with the help of two codes: Period04 [15] and Peranso V3.0.3.4 (www.cbabelgium.com/peranso). Both codes searched for significant peaks in the amplitude spectra using Fourier transformations of the light curves. Following the first frequency computation, we created the "periodogram"

by fitting a sinusoid to the Period04 period and subtracting the sinusoid from the original magnitude (pre-whitening). Then we calculate the periodogram again, but the first frequency will not be presented, so the highest peak in the periodogram will be the subsequent frequency. We repeated this procedure many times if necessary to search for other peaks until no more peaks could be seen in the periodogram. Results of our analysis presented in the Table 1. The sigma of the residuals is 6.747 mmag

Table 1

RESULTS OF FOURIER ANALYSIS APPLIED TO OUR DATA
SET OF KAO OBSERVATIONS

	Frequency (F) (c/d)	Amplitude (a) (mmag)	Phase (deg)	S/N
f_0	25.14427 ± 0.032979	157.193 ± 1.179	0.696 ± 0.001	85.50
$2f_0$		36.083 ± 1.180	0.750 ± 0.006	19.76
$3f_0$		7.4578 ± 1.199	0.928 ± 0.025	15.05
f_1	51.112 ± 0.0000342	14.762 ± 1.224	0.835 ± 0.013	64.30
f_2	33.3882934 ± 0.0000383	12.893 ± 1.211	0.732 ± 0.015	23.17
f_3	17.72464 ± 0.44729	11.590 ± 1.254	0.970 ± 0.016	41.90

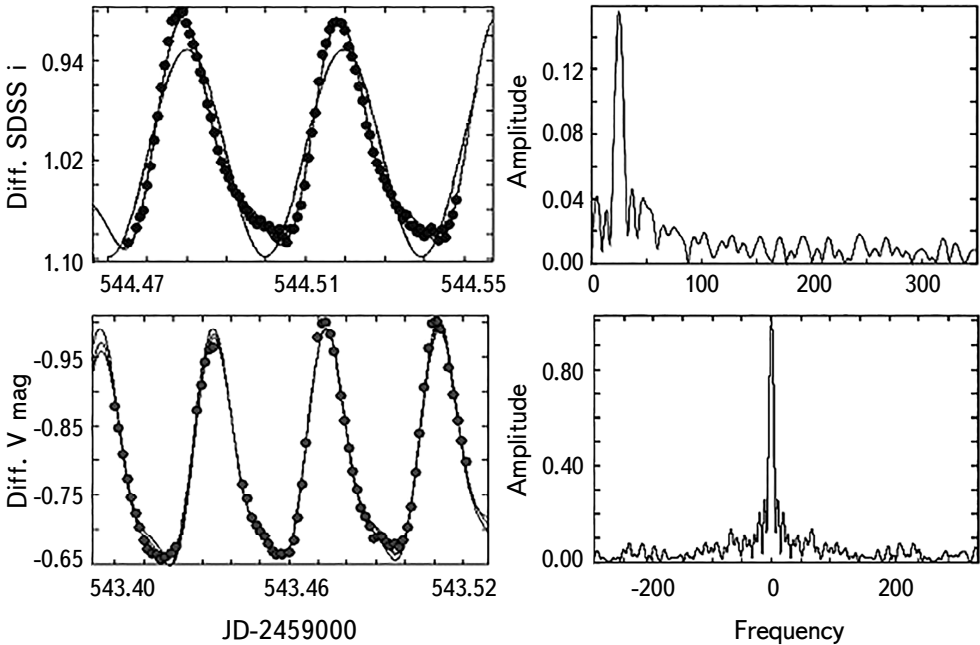


Fig.3. Observed light curves (left panel) represent the differential V and SDSS i magnitudes with the first frequency (25.5768439 c/d) in addition to other harmonics (solid lines), while the right panel is for the Fourier calculation using all data available from AAVSO and the spectral window in our observations.

The V-band light curve analysis reveals one peak in the periodogram at 0.03977049 d (25.1442704 ± 0.032979 c/d) (Fig.3).

We compared our results in Table 1 to that of [5], who used the data sets of [9,11] listed in Tables 5 and 6 together with the corresponding S/N values. Our results are in good agreement with those of [9]. The first impression from our results is; that we didn't find the secondary peak f_1 claimed by some authors in the region 31-32 c/d, [8] estimated f_1 as 32.6443 c/d, but we found the peak at 33.388 c/d. Also, we found a small difference between our f_0 (25.14427 c/d) and that of [7] (25.181 c/d) and [9] (25.5768 c/d). This difference may be attributed to our data being too short or not having enough data sets. In addition, independent frequencies f_2 and f_3 are detected together with the combinations $f_2 + f_3 \sim f_1 \sim 2f_0$, and the amplitudes of f_1 , f_2 , and f_3 are larger than $3f_0$. We do not detect at a significant level the linear combination $f_0 + f_1$ as reported by [9].

The sum of the squared residuals χ^2 derived from a multi-parameter least-squares fit of sinusoidal functions was used to calculate the error for each value. Fig.3 depicts the frequency spectra; Fourier fits on the observational points for all sets of observations and the spectral window of each star.

2.3. O-C curve and period change. We used the Hertzsprung [16] method to construct the O-C curve to determine the time of brightness minima or maxima. We used all the data published in the literature to fill in the gaps in the O-C diagram. We use it if the scatter is the same as the raw data (about 0.2 mag.). Fig.4 depicts the maximum-light times used to investigate the period change. To derive the O-C differences for BL Cam from a computed linear ephemeris, we used the method described by [16]. We establish a reference time of maximum light from existing photoelectric observations. The adopted pulsation period is based on recent observations of the star from KAO data. The following relationship gives the least-square fit by the quadratic elements:

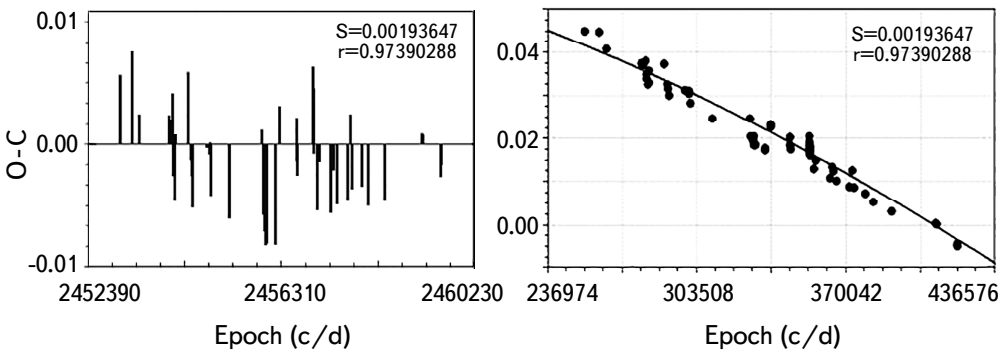


Fig.4. O-C data points fitted with a quadratic and the residuals of the quadratic fitting for BL Cam.

$$\text{HJD}_{\max} = M_0 + PE + QE^2, \quad (1)$$

where M_0 is a new epoch, P is the new period, and Q is used to measure the period change values (dP/dt) in seconds per year ($dP/dt = (2Q/P)365.25 \times 24 \times 60 \times 60$).

We employed a second-order polynomial least-squares approach to fit the O-C residuals. The revised ephemeris was evaluated using all available photometric observations from ASAS, KWS, and KAO to justify its validity throughout all observations. The linear ephemeris equation by [8] was used to calculate the light maximum

Table 2

THE NEW 55 TIMES OF MAXIMUM LIGHT, A NEW EPOCH, O-C,
NUMBER OF OBSERVATIONS, AND DATA SOURCE

HJD- 2450000	Epoch	O-C (days)	No. of Obs.	Ref.	HJD- 2450000	Epoch	O-C (days)	No. of Obs.	Ref.
3041.279	253607	0.04946	18	1	6186.419	334051	0.02209	60	1
3293.459	260057	0.04926	249	1	6186.458	334052	0.02170	56	1
3424.354	263405	0.04535	121	1	6280.259	336451	0.02717	35	1
4031.848	278943	0.04164	22	1	6280.298	336452	0.02776	40	1
4034.859	279020	0.04183	24	1	6623.336	345226	0.02268	262	1
4064.612	279781	0.04144	325	1	6623.375	345227	0.02287	220	1
4109.692	280934	0.04242	139	1	6623.416	345228	0.02483	255	1
4419.462	288857	0.04164	82	1	6630.372	345406	0.02189	201	1
4480.723	290424	0.03695	145	1	7034.402	355740	0.01740	28	2
4499.528	290905	0.03597	40	1	7074.440	356764	0.01935	44	1
4514.657	291292	0.03441	51	1	7314.652	362908	0.01525	58	2
4793.737	298430	0.03558	152	1	7362.901	364142	0.01779	48	1
4859.577	300114	0.03480	131	1	7370.719	364342	0.01681	48	2
4863.604	300217	0.03538	288	1	7437.457	366049	0.01466	37	2
4884.597	300754	0.03265	226	1	7651.398	371521	0.01329	37	2
5261.299	310389	0.02913	35	1	7715.639	373164	0.01701	133	1
5923.378	327323	0.02913	21	1	7745.935	373939	0.01310	47	2
5942.414	327810	0.02502	93	1	7942.947	378978	0.01173	41	2
5943.704	327843	0.02483	137	1	8077.636	382423	0.00977	39	2
5977.484	328707	0.02405	120	1	8394.755	390534	0.00762	35	2
5979.361	328755	0.02424	91	1	9168.884	410334	0.00469	60	1
5980.416	328782	0.02365	50	1	9177.642	410558	0.00450	93	1
5986.360	328934	0.02502	44	1	9543.434	419914	-0.00059	20	3
5993.357	329113	0.02326	42	1	9543.473	419915	-0.00039	17	3
5995.389	329165	0.02287	177	1	9543.512	419916	-0.00020	27	3
5996.367	329190	0.02346	156	1	9543.512	419916	-0.00020	7	3
6014.312	329649	0.02287	34	1	9544.529	419942	0.00000	90	3
6186.380	334050	0.02209	63	1					

1: AAVSO, 2: ASAS-SN, 3: KAO.

$$\text{HJD}_{\max} = 2443125.8026 + 0.03909783 E. \quad (2)$$

The 55 new times of maximum light obtained for BL Cam are presented in Table 2. The least-squares fit for O-C with the root mean square $R^2 = 0.954$ is

$$O-C = 7.994(14) \cdot 10^{-2} - 5.0349(15) \cdot 10^{-8} E - 3.2757(69) \cdot 10^{-13} E^2. \quad (3)$$

The quadratic trend in O-C data reflects a regular period decrease or increase. After constructing the O-C diagram, we found the decreasing period rate given by the equation

$$dp/dt = 0.17028E - 02 \pm 0.14378E - 05 \text{ s/yr}.$$

The standard deviation of the residuals of a quadratic fit to the O-C values is $0^d.002$, with a correlation coefficient of 0.97.

3. *Spectroscopic analysis.* We observed BL Cam covering the spectral ranges 3360-5870 Å and 5300-9180 Å, with spectral resolutions of ~ 1000 . The spectra were taken with the Kottamia Faint Imaging spectropolarimeter (KFISP) mounted on the 1.88 m telescope at Kottamia Astronomical Observatory (KAO) for a single night on November 25, 2021. The data were reduced using the Astropy-affiliated package CCDPROC [18]. We used the LACosmic routine [19] to remove cosmic rays from the images processed by Astro-SCRAPPY [20]. A particular Python routine was used to extract the spectra and calibrate the wavelength. Using IRAF, the spectra were flux calibrated. The signal-to-noise ratio was calculated with the specutils snr derived function [21]. Table 3 shows the log of the spectroscopic observations, and we plotted the BL Cam spectra in Fig.5. The upper panel represents the blue region, while the lower panel represents the red region.

We created a small grid of synthetic spectra from LTE model atmospheres with the effective temperature range of $6000 \leq T_{\text{eff}} \leq 10000$ K. We adopted ATLAS9 grids [22] as input models for LTE computations, assuming solar metallicity, a microturbulent velocity of 2 km/s, and a mixing length to scale height ratio of

Table 3

OBSERVATION LOG OF THE BL Cam SPECTRA

Time (UT)	HJD-2450000	Phase	Exposure (s)	Standard Star	λ Range	R	Airmass	Average S/N
21:29:32.96	9544.39554	0.376	900	HR9087	3360-5870	1025	1.198	113.9
21:59:40.35	9544.41644	0.939	900	HR9087	3360-5870	1025	1.206	113.3
22:25:30.52	9544.43438	0.406	900	HR9087	3360-5870	1025	1.220	105.5
23:01:03.12	9544.45906	0.931	900	HR9087	3360-5870	1025	1.252	108.0
21:17:03.84	9544.38687	0.598	600	HR9087	5300-9180	1133	1.198	146.0
21:48:45.29	9544.40886	0.133	600	HR9087	5300-9180	1133	1.202	166.2
22:15:05.11	9544.42714	0.592	600	HR9087	5300-9180	1133	1.213	159.0
22:44:36.40	9544.44764	0.223	600	HR9087	5300-9180	1133	1.235	189.6

1.25. The effective temperatures span the model grid's temperature range of 250 K. The surface gravities of the models are of $1 \leq \log g \leq 5$. We used the SPECTRUM code [23,24] to synthesize the LTE spectra (for the range $\lambda\lambda 1500-8000\text{\AA}$). SPECTRUM takes the depth points, temperatures, and total pressure and calculates them at each stage using a system of seven nonlinear equilibrium equations.

We developed a FORTRAN code that compares the flux values at each point on the observed and theoretical spectra. It then tabulates the differences to produce a single number that characterizes how good the fit is. The synthetic spectra are convolved with a Gaussian profile with $\text{FWHM} = 5\text{\AA}$. We adjusted the wavelength scale to begin comparing the observed and theoretical spectra. After that, we developed a code that minimizes the Euclidian distance between the observed and theoretical spectra to compare the grid with the observed spectra. The equivalent

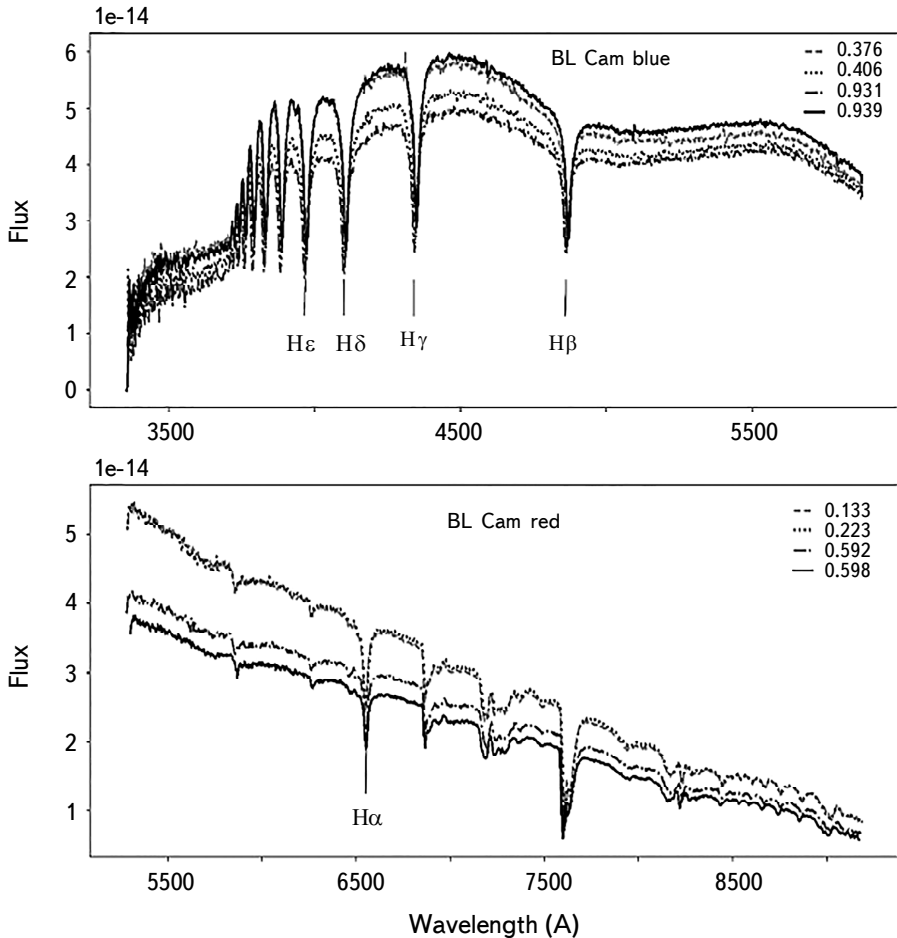


Fig.5. The observed spectra of BL Cam in the blue (upper panel) and red (lower panel) bands at different phases.

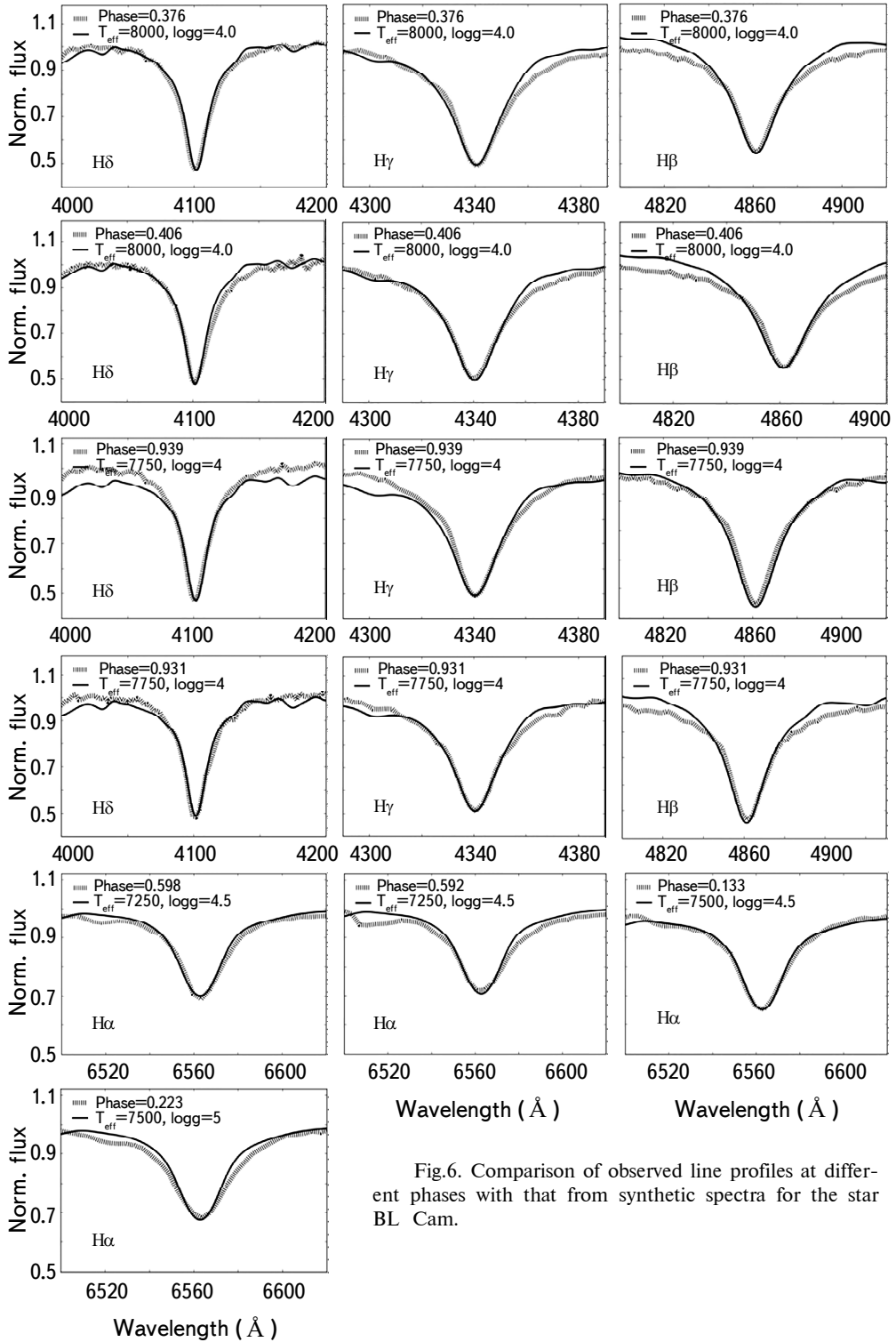


Fig.6. Comparison of observed line profiles at different phases with that from synthetic spectra for the star BL Cam.

Table 4

EFFECTIVE TEMPERATURES AND SURFACE GRAVITIES AT
DIFFERENT PHASES OF BL Cam

Phase	T_{eff} (K)	$\log g$
0.376	8000	4.0
0.406	8000	4.0
0.939	7750	4.0
0.931	7750	4.0
0.598	7250	4.5
0.592	7250	4.5
0.133	7500	4.5
0.233	7500	5.0
Mean	7625 ± 300	4.30 ± 0.37

widths of the spectral lines are calculated numerically using the Runge-Kutta technique.

Following the above procedure, we calculated the star's effective temperatures and surface gravities at different phases listed in Table 4. The mean effective temperature and surface gravity are adopted as $T_{eff} = 7625 \pm 300$ K and $\log g = 4.30 \pm 0.37$. Fig.6 shows the best fit of spectral lines H_{α} , H_{β} , H_{γ} , H_{δ} at different phases in both the red and blue parts of the spectrum. In most cases, we obtained a good fit for the line centers, while the significant difference between the observed and the synthetic spectra occurs for the line wings.

4. *Physical parameters and the evolution state.* We computed the physical parameters of BL Cam using the mean photometric colors, effective temperature, and the parallax. Adopting the effective temperature as $T_{eff} = 7625 \pm 300$ K, we calculated the bolometric correction as $BC = -0.089$ [25]; the star's absolute magnitude and bolometric magnitude in the visible filter as $M_v = 3.426 \pm 0.061$ and $M_{bol} = 3.337$.

The stellar radius is calculated from a polynomial fit to the temperature-radius relation of [23] as $R/R_{\odot} = 1.494 \pm 0.032$. The masses M can be calculated from the equation by [26] ($\log M = 0.46 - 0.10 M_{bol}$) as $M = 1.338 M_{\odot}$, and the luminosity is $L/L_{\odot} = 3.642$. The pulsational constant Q could be determined using the

Table 5

PHYSICAL PARAMETERS OF BL Cam

T_{eff} (K)	M/M_{\odot}	$\log L/L_{\odot}$	R/R_{\odot}	M_{bol}	$\log g$	Age(yr)	Q (days)
7625	1.68	0.957	1.69	2.335	4.3	2.295 Gy	0.025

frequencies in the periodogram (Table 1) from the equation

$$\log Q = 0.5 \log g + 0.1 M_{bol} + \log T_{eff} + \log P - 6.456. \quad (4)$$

Table 6

EFFECTIVE TEMPERATURES AND SURFACE GRAVITIES
OF SIX SX Phe STARS

Star name	T_{eff} (K)	logg	Ref.
SX Phe	7850	4.2	30
KZ Hya	7650	4	31
CY Aqr	7930	4.13	32
BS Tuc	7250	3.75	33
DY Peg	7800	4	32
XX Cyg	7530	3.66	34

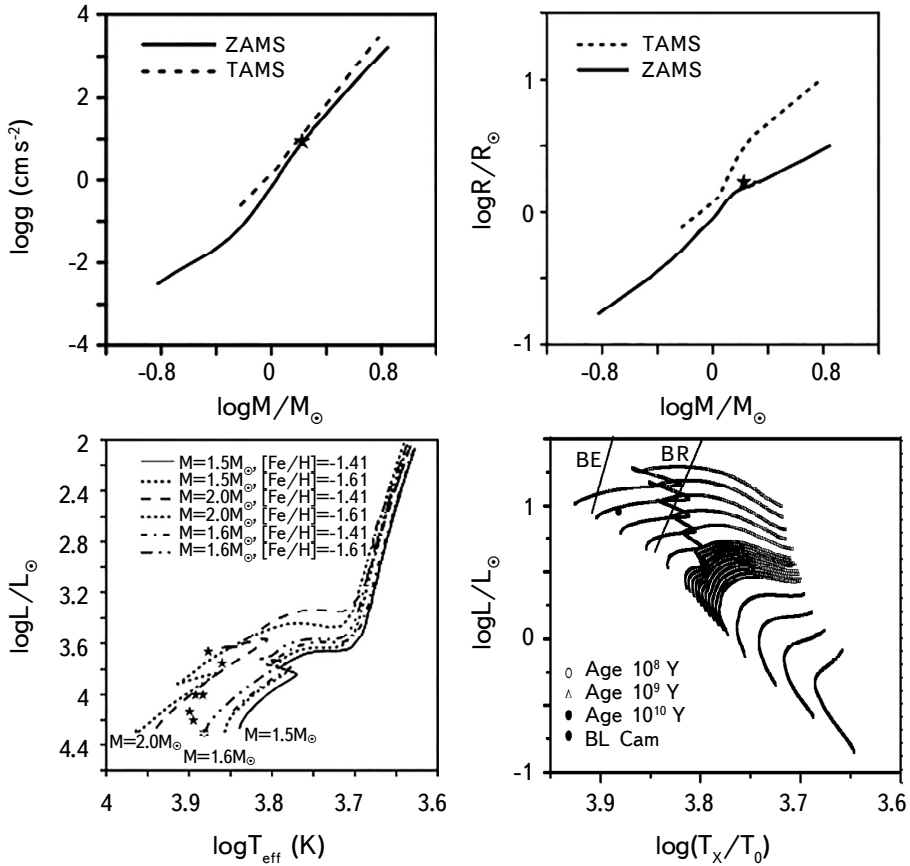


Fig.7. Locations of the BL Cam on the mass-luminosity (upper left panel) and temperature-radius (upper right panel) diagrams of [28] evolution models, and temperature-gravity (lower left panel), temperature-luminosity (lower right panel) of [28] evolution models for the metallicity $Z = 0.03$ (solid lines), and $Z = 0.019$ (dashed lines).

Consequently, the Q value of f_1 is 0.025(17), which is within the theoretical range, $0.0096 < Q < 0.067$, for the fundamental mode by [27]. The results are presented in Table 5; for the low-frequency pulsations ($\nu \leq 25$ c/d).

In Fig.7, we plotted the mass-luminosity relation ($M-L$) and mass-radius relation ($M-R$) for both zero-age main-sequence stars (ZAMS) and terminal-age main-sequence stars (TAMS) with metallicity $Z=0.014$ from the grid of [28]. The locations of BL Cam on the two diagrams are close to the ZAMS track, indicating an unevolved star.

Also, Fig.7 (lower left panel) illustrates the position of BL Cam and six SX Phe variables on the $\log T_{eff}-\log g$ diagrams for the mass tracks $1.4M_{\odot}-2M_{\odot}$. The parameters of BL Cam agree well with those predicted for SX Phe candidates listed in Table 6 [29]. The tracks are plotted for the metallicity values $Z=0.019$ ($[Fe/H] = -1.61$) and $Z=0.03$ ($[Fe/H] = -1.41$). In the lower right panel of Fig.8, we plotted the isochrones appropriate for the effective temperature and luminosity of BL Cam. In this figure, we can notice that the star crossed the instability strip's red edge (RE). From this diagram, the age of BL Cam could be determined as 2.295 GY.

5. Conclusion. We thoroughly analyzed the star BL Cam using photometric and spectroscopic observations obtained at the Kottamia observatory. According to the Fourier analysis of the light curves, the fundamental mode is independent pulsation mode at 25.14427 c/d and three harmonics, 51.112 c/d, 33.388 c/d, and 17.72464c/d. We combined the new times of maximum light with those provided by previous literature to perform an O-C analysis for the period change for BL Cam, yielding 55 times of maximum light. The variation rate of the fundamental period derived from the long-time scale of observations shows a negative period change ($dp/dt = 0.17028 E-02 \pm 0.14 E-05$ s/yr).

We used LTE model atmospheres to simulate the observed spectra. The effective temperatures and surface gravities at different phases are calculated by comparing the spectra to the appropriate synthetic spectra. We adopted the effective temperature and surface gravity of BL Cam as $T_{eff} = 7625 \pm 300$ K and $\log g = 4.30 \pm 0.37$, which is in good agreement with earlier studies. We located the star's physical parameters on the evolutionary models to investigate its evolution state. The calculated mass ($1.68 M_{\odot}$) is in good agreement with mass tracks around $1.6 M_{\odot}$ and higher than the possible masses ($1.0 M_{\odot}-1.4 M_{\odot}$) of the SX Phe stars predicted by [29].

Acknowledgments. This paper is based upon work supported by Science, Technology & Innovation Funding Authority (STDF) under grant number 45779. We appreciate the editor's, the reviewers' valuable comments and suggestions which helped the authors improve the manuscript.

ФОТОМЕТРИЧЕСКИЙ И СПЕКТРОСКОПИЧЕСКИЙ АНАЛИЗ ЗВЕЗДЫ ТИПА SX Phe BL Cam

М.АБДЕЛ-САБУР, М.И.НОУ, А.ШОКРИ, Г.М.ХАМЕД,
Х.А.ИСМАИЛ, А.ТАКЕЙ, С.А.АТА, И.ЗЕАД

В настоящей работе представлены фотометрические и спектроскопические наблюдения пульсирующей звезды BL Cam, полученные 1.88-метровым телескопом в астрономической обсерватории Коттамия (КАО). Фурье-анализ кривых блеска показывает частоту 25.14427 ц/сут, с гармониками 51.112 ц/сут, 33.388 ц/сут и 17.72464 ц/сут. Частота 31-32 ц/сут, о которой сообщается в литературе, не обнаружена в наших данных, за исключением частоты, близкой к 33.3882934 ц/сут. В общей сложности представлено 55 новых максимумов блеска. Новое значение $(1/P) dP/dt$ оценивается с использованием диаграммы О-С, основанной на всех вновь полученных временах максимумов в сочетании с периодами, взятыми из литературы, предполагая, что периоды уменьшаются и изменяются плавно. Используя модельный анализ атмосферы, вычислены эффективная температура и ускорение силы тяжести $T_{eff} = 7625 \pm 300$ К и $\log g = 4.30 \pm 0.37$ dex. Боллометрическая величина $M_{bol} = 2.335$, радиус $R = 1.69 R_{\odot}$, светимость $L = 0.957 L_{\odot}$, масса $M = 1.68 M_{\odot}$, константа пульсации $Q = 0.025$ сут. Расположение звезды на диаграммах $M-R$ и $M-L$ указывает на то, что она находится близко к ZAMS и является не эволюционировавшей звездой.

Ключевые слова: *звезды: переменные: звезды типа SX Phe: частотный анализ пульсаций: анализ моделей атмосфер*

REFERENCES

1. P.Zong, A.Esamdin, J.N.Fu et al., Publ. Astron. Soc. Pacif., **131**, 4202, 2019.
2. H.L.Giclas, R.Burnham, N.G.Thomas, Lowell Observatory Bulletin, **7**, 183, 1970.
3. R.A.Berg, J.G.Duthie, Astrophys. J. Lett., **215**, L25, 1977.
4. D.McNamara, Publ. Astron. Soc. Pacif., **109**, 1221, 1997.
5. S.Fauvaud, E.Rodriguez, A.Y.Zhou et al., Astron. Astrophys., **451**, 999, 2006.
6. E.Rodriguez, S.Fauvaud, J.A.Farrell et al., Astron. Astrophys., **471**, 255, 2007.
7. J.-N.Fu, C.Zhang, K.Marak et al., ChJAA, **8**, 237, 2008.
8. E.G.Hintz, M.D.Joner, D.H.McNamara et al., Publ. Astron. Soc. Pacif., **109**, 15, 1997.
9. A.-Y.Zhou, E.Rodriguez, S.-Y.Jiang et al., Mon. Not. Roy. Astron. Soc., **308**,

- 631, 1999.
10. *C.Kim, E.-J.Sim*, JASS, **16**, 241, 1999.
 11. *A.-Y.Zhou, B.-T.Du, X.-B.Zhang et al.*, IBVS, **5061**, 1, 2001.
 12. *M.Wolf, M.Crlikova, M.Basta et al.*, IBVS, **5317**, 1, 2002.
 13. *J.H.Pena, J.D.Paredes, D.S.Piña et al.*, Revista Mexicana de Astronomía y Astrofísica, **57**, 419, 2021.
 14. *F.Hroch*, Proceedings of the 29th Conference on Variable Star Research, 30, 1998.
 15. *P.Lenz, M.Breger*, Communications in Asteroseismology, **146**, 53, 2005.
 16. *E.Hertzprung*, BAN, **4**, 178, 1928.
 17. *M.Abdel-Sabour, A.Shokry, A.Ibrahim*, Revista Mexicana de Astronomía y Astrofísica, **56**, 287, 2020.
 18. *M.Craig, S.Crawford, M.Seifert et al.*, astropy/ccdproc: v1.3.0.post1, doi:10.5281/zenodo.1069648. <https://doi.org/10.5281/zenodo.1069648>, 2017.
 19. *P. van Dokkum*, Publ. Astron. Soc. Pacif., **113**, 1420, 2001.
 20. *C.McCully, S.Crawford, G.Kovacs et al.*, astropy/astroscrappy: v1.0.5 Zenodo Release, <https://zenodo.org/record/1482019>, 2018.
 21. *N.Earl, E.Tollerud, C.Jones et al.*, astropy/specutils: V1.5.0, v1.5.0, Zenodo, doi: 10.5281/zenodo.5721652, 2021.
 22. *R.L.Kurucz*, HiA, **10**, 407, 1995.
 23. *R.O.Gray*, Astron. Astrophys., **265**, 704, 1992.
 24. *R.O.Gray*, Astron. Astrophys., **273**, 349, 1993.
 25. *C.B.Reed*, Astrophys. J. Suppl. Ser., **115**, 271, 1998.
 26. *A.N.Cox*, Proceedings of IAU Colloq. 111, held in Lincoln, NE, 15-17 August 1988. Edited by E.G.Schmidt, Cambridge Univ. Press.; p.1, 1989.
 27. *W.S.Fitch*, Proceedings of the Workshop, Tucson, Ariz., March 12-16, 1979. (A81-21401 07-90) Berlin, Springer-Verlag;; p.7-21, 1980.
 28. *L.Girardi, A.Bressan, G.Bretelli et al.*, Astrophys. J. Suppl. Ser., **141**, 371, 2000.
 29. *J.Nemec, M.Mateo*, in C.Cacciari, G.Clementini, eds, Astronomical Society of the Pacific Conference Series Vol. 11, Confrontation Between Stellar Pulsation and Evolution, p.64-84, 1990.
 30. *M.S.Bessel*, Astrophys. J. Suppl. Ser., **18**, 195, 1969.
 31. *A.Przybylski, M.S.Bessell*, Mon. Not. Roy. Astron. Soc., **189**, 377, 1979.
 32. *D.H.McNamara, A.K.Feltz*, Publ. Astron. Soc. Pacif., **90**, 275, 1978.
 33. *A.W.Rodgers*, Astrophys. J., **152**, 109, 1968.
 34. *M.D.Joner*, Publ. Astron. Soc. Pacif., **94**, 289, 1982.